PHYSICAL REVIEW B **81**, 085420 (2010)

Ultrasensitive detection of lateral atomic-scale interactions on graphite (0001) via bimodal dynamic force measurements

Shigeki Kawai,* Thilo Glatzel, Sascha Koch, Bartosz Such,† Alexis Baratoff, and Ernst Meyer
Department of Physics, University of Basel, Klingelbergstr. 82, 4056 Basel, Switzerland
(Received 11 December 2009; published 17 February 2010)

Enhanced sensitivity to lateral forces on the nominally flat and inert (0001) surface of graphite is demonstrated via room-temperature dynamic force microscopy using simultaneous excitation and FM detection of the lowest flexural and torsional cantilever resonance modes. The site-independent long-range tip-sample interaction causes no significant lateral force variations except near atomic steps but unprecedented sensitivity to short-range forces is achieved on flat terraces in the attractive range. Two-dimensional bimodal force vs distance maps confirm the stronger distance dependence of the torsional frequency shift compared to the flexural resonance shift. This agrees with model calculations based on theoretical expressions. The lateral force gradient is extracted from the measured torsional shift, and a lateral force variation in at most ± 20 pN is obtained by integrating this gradient parallel to the surface. A further integration reveals a potential-energy variation in the attractive force range of only 3 meV.

DOI: 10.1103/PhysRevB.81.085420 PACS number(s): 07.79.Lh, 34.20.Cf, 68.37.Ps

I. INTRODUCTION

Carbon is one of the most fundamental elements, especially in organic materials,[1] and usually bonds strongly to neighboring atoms. The resulting sp^2 covalently bonded structures are very robust and their surfaces are usually inert. Graphite is the prototypical such material and has a laminated structure. Since graphite layers are weakly bonded to each other by van der Waals interaction, the surface layer is extremely soft in the vertical direction. This feature hinders stable imaging with atomic resolution by dynamic force microscopy (DFM), especially at room temperature (RT). In conventional frequency demodulation DFM, vertical interactions between tip and sample shift the flexural resonance frequency of an oscillating cantilever, and the tip-sample distance is controlled by keeping a constant frequency shift.[2] In order to detect atomic-scale variations in the tip-sample interaction, the tip apex should come as close as possible to the sample surface. However, due to easy vertical deformations of the graphite surface, instabilities are difficult to avoid, and stable imaging with atomic resolution has so far succeeded only at low temperature.[3–8] Such deformations usually produce a *giant corrugation* first detected in scanning tunneling microscopy,[9,10] and only recently in DFM.[11] However, owing to the unusually high lateral stiffness of graphite layers, lattice imaging in contact-mode atomic force microscopy is routinely obtained.[12]

The lateral interactions are recently detected by the dynamic response of an oscillating cantilever. Dynamic lateral force microscopy[13–16] is a very promising technique to enhance the detection sensitivity to lateral forces. In this mode, the tip is forced to oscillate parallel to the sample surface by driving a rectangular Si cantilever at its lowest torsional resonance frequency, and the lateral force gradient between tip and sample is detected from the resonance frequency shift.[13,15,16] Since at the atomic scale, the lateral force gradient is periodically modulated, hence change sign along the surface, the torsional frequency shift cannot be used for tip-sample distance regulation,[16] and hence the tunneling current has been used for that purpose.[13,14,16] When a rectangular Si cantilever is used as a force sensor, the tip-apex oscillation parallel to the sample surface can be kept small because the high mechanical quality factor above 100 000 and the high resonance frequency above 1 MHz of the torsional resonance enhance the detection sensitivity.[2] However, since the tip apex is not deflected in the vertical direction, as with soft cantilevers used in contact-mode force microscopy, the time-averaged lateral force caused by scanning the tip too close to the surface can significantly deform the sample or the tip.[16,17] Especially in the case of graphite since the tip apex is typically in the repulsive range at tunneling distances, the influence of surface deformations is not clear.[11] In order to avoid lateral deformations, the stored deformation energy must be released at each measurement point so that sufficient vertical tip movement is mandatory.

Recently, improved imaging using bimodal DFM (Refs. 18–20) has been demonstrated, mainly at scales of nanometers and above under environmental conditions. In this technique, two resonance modes of a Si cantilever are simultaneously excited. The first resonance is used for tip-sample distance control, often in the repulsive range, and the second resonance is used for the detection of surface mechanical, adhesive, electric, or magnetic properties of heterogeneous materials. Bimodal DFM can also be applied for atomic-scale imaging in the noncontact region.[21] We found that for small second-mode amplitudes (<100 pm), the detection sensitivity in the second flexural resonance frequency shift is even higher than that in the first one. Actually, the detection sensitivity is worse than that in principle achievable using small amplitude DFM with a single mode alone[22–25] but a large amplitude of the first-flexural mode ensures stable imaging even at surfaces of soft materials, such as KBr(001).[21]

In the present paper, we present and interpret atomically-resolved bimodal DFM measurements using the lowest flexural and torsional resonance modes on graphite (0001). A large amplitude of the first-flexural resonance mode, oscillating in the vertical direction, eliminates unwanted lateral deformations of tip and sample. A small amplitude of the tor-

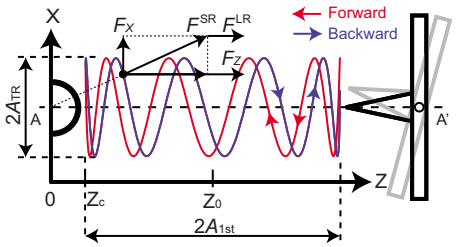

FIG. 1. (Color online) Schematic drawing of tip and sample in bimodal DFM with the first-flexural and torsional resonances modes. The lines and the arrows show the tip trajectories during oscillations toward and away from the sample, respectively.

sional resonance mode enables sensitive detection of lateral interactions in a range where none are seen in conventional DFM, except in the vicinity of the top layer exposed at steps. Since the site-independent long-range interaction causes no lateral forces, the strong distance dependence of short-range forces leads to an extremely high spatial resolution in the torsional resonance frequency shift map with a sub-angstrom amplitude.

II. THEORY AND SIMULATIONS

Figure 1 shows a schematic view along the cantilever axis illustrating the tip trajectory in bimodal DFM with the first-flexural and torsional resonance modes. Since the maximum twist angle of a Si cantilever in the torsional resonance mode is very small, the tip apex moves parallel to the sample surface and accurately senses the local lateral interaction force between tip and sample.[13,15,16] The direction of the lateral tip movement is defined as X. The first-flexural f_{1st} and torsional resonance frequencies f_{TR} are incommensurate so that the trajectory during the oscillation cycle of the flexural resonance mode differs when the tip apex moves toward and away from the sample. In the next oscillation cycle, the tip trajectory also deviates from the previous one. Due to the finite measurement bandwidth of around several 100 Hz, a typical cantilever with f_{1st} of $\approx$150 kHz and f_{TR} of $\approx$1.5 MHz oscillates about 1500 cycles in the vertical direction and about 15 000 cycles in the lateral direction at each recording point. At each point of the oscillation, the short-range interaction force F_{SR} can be divided into vertical F_Z and lateral components F_X. The site-independent long-range interaction force F_{LR} only contributes to the vertical F_Z. Assuming that these forces weakly perturb the independent harmonic oscillations in each mode, the frequency shifts of the first-flexural Δf_{1st} and torsional resonance modes Δf_{TR} are given by

$$k_i \frac{\Delta f_i}{f_i} = \frac{1}{2\pi A_i n_i} \int_0^{2\pi n_i} F_j[\mathrm{tip}(X,Z)] \cos\,\theta_i d\theta_i, \qquad (1)$$

where k_i is the effective stiffness, Δf_i the shift of the resonance frequency f_i, A_i the amplitude, and n_i the large number of the oscillation cycles of mode i while F_j is the interaction force component in direction j (X denotes the lateral direction and Z the vertical direction), and tip(X,Z) is the tip-apex position in the X-Z plane. In order to reliably sample the interaction over time, the numbers n_i must also be chosen large in simulations (typically above 100 for Δf_{1st} and above 2000 for Δf_{TR}). The position of the tip apex in the X-Z plane can be described as

$$\mathrm{tip}(X,Z) = (A_{TR} \cos\,\theta_{TR}, Z_0 + A_{1st} \cos\,\theta_{1st}), \qquad (2)$$

where Z_0 is the equilibrium tip-sample distance, $\theta_{TR} = 2\pi f_{TR} t$, $\theta_{1st} = 2\pi f_{1st} t$, and t the time. To avoid averaging of the lateral forces at the atomic scale, the amplitude of the torsional resonance A_{TR} mode has to be set small compared to interatomic atomic distances.[26] Hereafter, the theoretical discussion will be based on this condition. Then Δf_{1st} is still given by the well-known expression,

$$k_{1st} \frac{\Delta f_{1st}}{f_{1st}} = \frac{1}{2\pi A_{1st}} \int_0^{2\pi} F_Z(Z_0 + A_{1st} \cos\,\theta) \cos\,\theta d\theta, \qquad (3)$$

valid as long as $\Delta f_{1st}/f_{1st} \ll 1$ for monomodal DFM.[27,28] For amplitudes A_{1st} of the first-flexural resonance mode much larger than the decay length λ of the short-range interaction (typically $A_{1st} > 10$ nm), Eq. (3) can be further approximated as

$$k_{1st} \frac{\Delta f_{1st}}{f_{1st}} = -\frac{1}{2\pi A_{1st}} \int_0^{2\pi} F_Z(Z_0 + A_{1st} \cos\,\theta) d\theta \qquad (4)$$

because most of the contribution to the integral comes from the turning point where $\cos\,\theta_{1st} \approx -1$.

Recently, we studied in detail atomic-scale bimodal DFM using the first-flexural and second-flexural resonance modes.[21] In particular, the following expression for the frequency shift of the second-flexural mode Δf_{2nd} was derived if the conditions $A_{1st} \gg \lambda > A_{2nd}$ are satisfied,

$$k_{2nd} \frac{\Delta f_{2nd}}{f_{2nd}} = -\frac{1}{4\pi} \int_0^{2\pi} F'_Z(Z_0 + A_{1st} \cos\,\theta) d\theta, \qquad (5)$$

where F'_Z is the vertical interaction force gradient. Analysis of Eqs. (4) and (5) shows that since this gradient is more sensitive to short-range interactions than the force itself, Δf_{2nd} has a stronger distance dependence than Δf_{1st}, hence exhibits a higher spatial resolution for a given A_{1st}.[21]

In a similar manner, the shift Δf_{TR} in bimodal DFM using the first-flexural and torsional resonance modes under the stated conditions $A_{1st} \gg \lambda > A_{TR}$ is given by

$$k_{TR} \frac{\Delta f_{TR}}{f_{TR}} = -\frac{1}{4\pi} \int_0^{2\pi} F'_X(Z_0 + A_{1st} \cos\,\theta) d\theta, \qquad (6)$$

where F'_X is the lateral interaction force gradient in the X direction.

The validity of the approximations made in deriving Eq. (6) is now tested using the following simple model. A single atom is considered on the sample surface, and the short-range and long-range interactions between tip and sample are modeled by Morse-type[29] and Hamaker-type forces[30] along the trajectory A-A′ shown in Fig. 1. Figure 2(a) shows the assumed interaction forces. The Morse force describing the interaction between a Si dangling bond and a Si adatom[29] is given by $F_{sr} = 2E_{sr}/\lambda\{\exp[-2(r-\rho)/\lambda] - \exp[-(r-\rho)/\lambda]\}$, E_{sr}

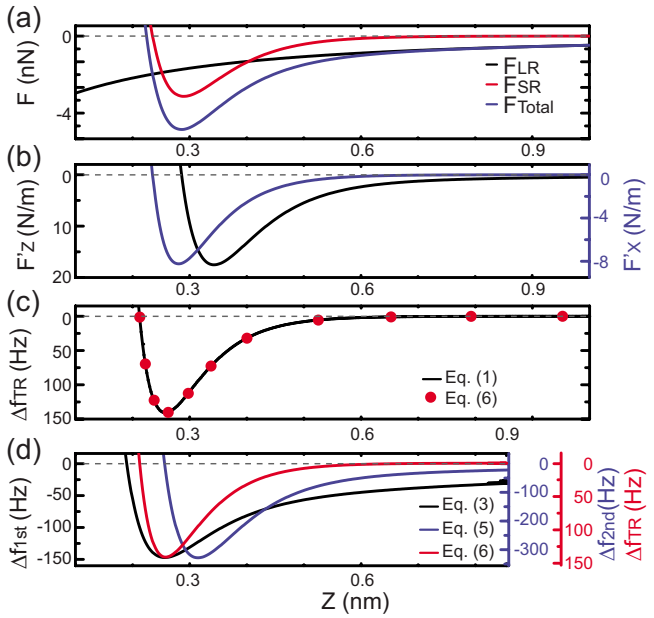

FIG. 2. (Color online) Distance dependence of (a) the long-range force F_{LR}, the vertical short-range force F_{SR}, and total interaction force F_{Total} along A-A′ in Fig. 1, and (b) vertical F'_Z and lateral force gradients F'_X all calculated with an assumed model tip-sample interaction potential (see text). (c) Frequency shift Δf_{TR} of the torsional resonance computed with Eq. (1) (points) and Eq. (6) (curve). (d) Computed frequency shifts Δf_{1st}, Δf_{2nd} of the first- and second-flexural modes, and of the first torsional resonance, Δf_{TR}, using Eqs. (3), (5), and (6), respectively. Assumed parameters: $f_{1st}=150$ kHz, $f_{2nd}=980$ kHz, $f_{TR}=1480$ kHz, $k_{1st}=25$ N/m, $k_{2nd}=1450$ N/m, $k_{TR}=2000$ N/m, $A_{1st}=10$ nm, $A_{TR}=10$ pm, $R_{tip}=5$ nm, and $\lambda=79$ pm.

being the binding energy (2.27 eV), λ the characteristic range (79 pm), and ρ the location of the potential minimum along the apex-atom axis (235 pm), respectively. The long-range van der Waals force is described as $F_{vdW}=-A_H R_{tip}/(Z+Z_{off})^2$, A_H being the Hamaker constant (≈ 1 eV) for Si,[31] R_{tip} the assumed mesoscopic tip radius (5 nm), and Z_{off} an origin offset[30] with respect to the short-range interaction (500 pm). Figure 2(b) shows the vertical F'_Z and lateral F'_X force gradients calculated by differentiating the interaction force in X and Z directions at each tip-sample distance, respectively. Just aside the atom in our simple model, the lateral force is

$$F_X \approx F_{sr}(\sqrt{Z^2+X^2})\frac{X}{\sqrt{Z^2+X^2}} \tag{7}$$

and its gradient is simply $F'_X=F_{sr}/Z$. Since only the site-dependent short-range interaction contributes to the lateral force, the calculated lateral gradient has a stronger distance dependence than the total vertical gradient. It is worth mentioning that the distance dependence of the vertical force gradient is the same as that of the flexural frequency shift in the ultrasmall amplitude limit ($\Delta f=-F'_Z f/2k$).[2] The validity of the assumptions made to derive Eq. (6) is verified by computing Δf_{TR} with Eqs. (1) and (6), separately [Fig. 2(c)]. A_{TR} was set 10 pm, and the lateral interaction was integrated over 400 oscillation cycles of the first-flexural resonance mode with an amplitude of 10 nm. The points computed using Eq. (6) are in excellent agreement with the direct calculation using Eq. (1). Although the tip oscillates with a large A_{1st} in the vertical direction, the calculated Δf_{TR} follows the lateral force gradient, shown in Fig. 2(b), mainly due to the strong distance dependence of the lateral force gradient. The tip-sample distance corresponding to the most positive Δf_{TR} is shifted by only ≈ 80 pm toward to the sample surface with respect to the maximum F'_X.

Next, we compare the detection sensitivities of Δf_{2nd} and Δf_{TR} in bimodal DFM with large A_{1st}. The only difference between Eqs. (5) and (6) is the direction of the force gradient. Because Δf_{TR} arises only from the site-dependent interactions, the macroscopic shape of the tip apex should not, in principle, affect the lateral force detection as long as stable imaging remains possible. The sensitivity should be extremely high, and better than what could be achieved even with ultrasmall amplitude DFM using a flexural mode,[23,32] owing to the nonzero contribution of the long-range interaction. In Fig. 2(d), the maximum Δf_{TR} is about half the maximum of Δf_{2nd} with the assumed parameters but because the mechanical quality factor of the torsional-mode Q_{TR} is typically ten times higher than that of the second-flexural mode Q_{2nd}, the resulting signal/noise ratio should nevertheless be better.

III. EXPERIMENTAL

All experiments were performed with our homemade ultrahigh-vacuum DFM, operating at RT.[33] The graphite (0001) surface was obtained by cleaving a highly ordered pyrolytic graphite (HOPG) sample with adhesive tape in air, rapid transfer into the vacuum chamber, and then annealing at 250 °C to remove contaminants on the surface. A commercially available Si cantilever (Nanosensor NCL-PPP) was used to detect the vertical and lateral interactions between tip and sample. The cantilever was annealed at 150 °C in the preparation chamber and the tip was then cleaned by Ar^+ sputtering. The tip-sample distance was controlled by keeping a constant negative Δf_{1st}, and the lateral force gradient was simultaneously detected via Δf_{TR}. The f_{1st} and f_{TR} signals were demodulated by two separate phase-locked loop circuits (Nanonis Dual-OC4), and both A_{1st} and A_{TR} were kept constant with automatic gain controllers. A_{1st} was set above 10 nm and A_{TR} was set below 100 pm A_{1st} was calibrated using the "constant γ method" in the amplitude range of 10 ± 2 nm.[34] A_{TR} was calibrated with the observed periodicity of the Δf_{TR} map, as explained in detail elsewhere.[35] In order to achieve tip movement parallel to the sample surface, the angle of the sample with respect to the cantilever width was adjusted by the coarse sample piezoactuator. The remaining misalignment measured using the tilt angle correction of the scanning probe software was quite small (1.3°). The sample was voltage biased with respect to the tip in order to approximately minimize long-range electrostatic forces. Recorded data were analyzed using the WSXM software,[36] and thermal drifts in the images were corrected *a posteriori*.

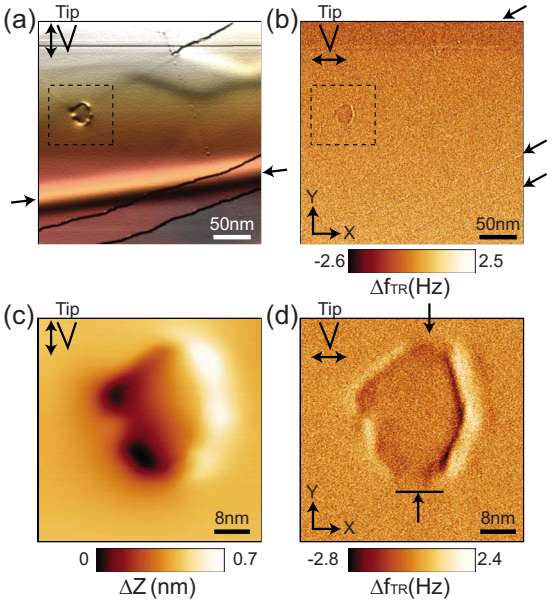

FIG. 3. (Color online) (a) Topography and (b) Δf_{TR} map of graphite (0001) in a scan area of 300 nm$\times$300 nm. (c) Topography and (d) Δf_{TR} map inside the dashed square around the pit observed in (a); the scan area is 50 nm$\times$50 nm. Double-headed arrows schematically depict the directions of the tip oscillations used to record the data. The significance of the other arrows is discussed in the text. Imaging parameters; (a) and (b) $\Delta f_{1\mathrm{st}}$=−19.8 Hz, $A_{1\mathrm{st}}$=10 nm, A_{TR}=38 pm, the sample bias V_{bias}=0.244 V. (c) and (d) $\Delta f_{1\mathrm{st}}$=−20.0 Hz, $A_{1\mathrm{st}}$=15 nm, A_{TR}=63 pm, V_{bias}=0.464 V. $f_{1\mathrm{st}}$=152297 Hz, f_{TR}=1493393 Hz, $Q_{1\mathrm{st}}$=34994, and Q_{TR}=135109.

IV. RESULTS AND DISCUSSIONS

Figure 3(a) shows the topography of graphite (0001) over a large area of 300 nm$\times$300 nm. apart from atomic steps highlighted by black lines, a wavy feature is observed in the lower part of the image between the two side arrows, and similar features are also observed in the top part. They may be induced by a partial detachment of the top layer from the underlying graphite layers. Following cleavage, exfoliated graphite flakes often cover the surface, another indication of the weak bonding between layers. Within the drawn dashed square, a pit is observed. The simultaneously recorded Δf_{TR} map shown in Fig. 3(b) reveals no corrugation on the flat parts, except for weak, but visible features at the edges of the pit and at the steps, indicated by the arrows on the left side. Figure 3(c) shows a zoomed topography of the pit. Although the surface around the pit belongs to the same graphite layer, the surface near the right edge appears to protrude both in Figs. 3(c) and 3(d). Presumably a part of the exposed layer at that edge was lifted and also oscillated laterally during the bimodal measurement. As explained in Sec. II, the Δf_{TR} is proportional to the time-averaged lateral force gradient in the X direction [Eq. (6)]. Any lateral interaction in the Y direction is insensitive to the dither applied in the X direction indicated the double-headed arrow in Fig. 3(d). While at the left and right sides of the pit, large modulations of Δf_{TR} were observed, almost no modulation was observed at the top and bottom sides.

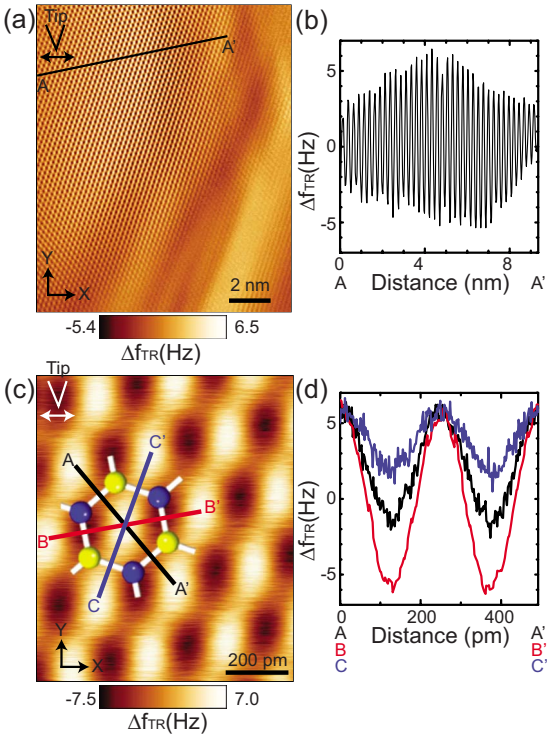

FIG. 4. (Color online) (a) Δf_{TR} map near the left side of the pit in Fig. 3(d) in a scan area of 15 nm$\times$15 nm and (b) corresponding line profile along A-A′. (c) Δf_{TR} map on the flat part in a scan area of 810 pm$\times$970 pm together with a superposed carbon hexagon properly placed with respect to the surrounding maxima (hollow sites), and (d) corresponding line profiles along A-A′, B-B′, and C-C′. Imaging parameters; $\Delta f_{1\mathrm{st}}$=−248 Hz in (a) and $\Delta f_{1\mathrm{st}}$=−249 Hz in (c), $A_{1\mathrm{st}}$=15 nm, A_{TR}=63 pm, and V_{bias}=0.265 V.

Figure 4(a) shows a Δf_{TR} map recorded near the left side of the pit in a scan area of 15 nm$\times$15 nm. A clear atomic-scale periodicity close to the distance between neighboring hollow sites (246 pm) is observed. Due to the close correspondence between the interatomic distance of carbon atoms in graphite layers (142 pm) and the decay length of the short-range interaction, the vertical tip-sample interaction force in the attractive range is strongest at the hollow sites,[37] and consequently those sites are observed as a maxima in conventional DFM.[38] In the attractive range, the hollow site can therefore be considered as equivalent to the atom in the simple model discussed in Sec. II. Hence, the most negative lateral interaction force gradient and, according to Eq. (6), the most positive Δf_{TR} are realized at this site. Therefore, the observed protrusions in Fig. 4(a) are the hollow sites. Figure 4(b) shows a line profile of Δf_{TR} along A-A′. The amplitude of the sinusoidal Δf_{TR} signal is slowly modulated over the measured area while the baseline remains constant. On the upper terrace near the pit edge, the graphite surface layer can easily move up and down. As a consequence, the tip-sample distance in a constant $\Delta f_{1\mathrm{st}}$ mode is modulated and the ratio of the short-range and long-range interactions can change. Since the distance dependence of the lateral force gradient is very strong, small changes in the tip-sample distance can be observed with enhanced contrast in the modulation envelope of Δf_{TR}.

Figure 4(c) shows a high-resolution Δf_{TR} image in a scan area of 810 pm × 970 pm on a topographically flat region. A schematic drawing of a graphite-carbon hexagon ring superposed. Its orientation was determined as follows. Due to the anisotropic detection of the lateral force gradient by the tip dither in the X direction, the observed corrugation appears extended in the Y direction. This feature is consistent with similar observations on the Si(111)-7×7 surface.[16] Since no corresponding feature was observed in the topography (not shown), the detected Δf_{TR} can be regarded as the lateral force gradient in the X direction time averaged over a large A_{1st} oscillation at a *de facto* constant height. Based on the relation between the vertical and lateral forces described by Eq. (7), a large positive Δf_{TR} is detected over the hollow site. The most negative Δf_{TR} should be detected over the bridge site halfway between neighboring α and β carbon-site atoms, if the dithering direction of the tip apex were perpendicular to the bridge direction. However, since the dithering direction is fixed in the measurement, the detection sensitivity of the lateral force gradient changes with the direction of α and β bonds with respect to the dithering direction. This change is clearly observed in the line profiles along A-A′, B-B′, and C-C′, shown in Fig. 4(d). All three Δf_{TR} line profiles are sinusoidally modulated but the offset and the amplitude change systematically. Since the three lines are running along equivalent symmetry axes, the tip feels identical vertical interaction forces, and therefore, the differences of the detected Δf_{TR} are mainly due to the angles with respect to the dithering direction X. The largest modulation of Δf_{TR} with a zero-offset frequency shift is observed along B-B′ because this line is almost parallel to X. With increasing angle, the offset Δf_{TR} becomes more positive and the modulation amplitude becomes smaller.

In order to investigate the spatial dependence of Δf_{TR} in more detail, a two-dimensional (X-Z) mapping was performed by bimodal dynamic force spectroscopy (DFS) measurements at 256 equally spaced positions in the X direction. After each Z distance-dependence measurement, the tip-sample distance was readjusted at a constant Δf_{1st} of −19.0 Hz. The origin of the Z axis was arbitrarily set to the closest tip-sample distance. Since the bimodal DFS measurement took 64 min, unavoidable thermal drifts at RT made the actual X and Y positions of the tip apex uncertain. However, since the thermal drift in the Z direction was only 207 pm over the measurement time, the resulting drift should be even smaller in the X direction. Figure 5(a) shows the two-dimensional Δf_{1st} map in the X-Z plane over the flat terrace. No significant atomic contrast is observed and Δf_{1st} monotonically becomes more negative with decreasing the tip-sample distance. With A_{1st}=15 nm, the detection sensitivity was not high enough to detect any lateral variation in the interaction via Δf_{1st}. The inset shows the vertical interaction force extracted from the measured Δf_{1st}, using Sader and Jarvis's algorithm.[39] However, a clear atomic contrast is observed in the Δf_{TR} map [Fig. 5(b)]. At tip-sample distances above 0.7 nm, no Δf_{TR} signal is detected. Then down to 0.3 nm, weak but detectable atomic-scale variations are observed. Below 0.3 nm, a high contrast pattern tilted with respect to the direction normal to the surface is observed, especially in the magnified inset. A finite tilt angle of the

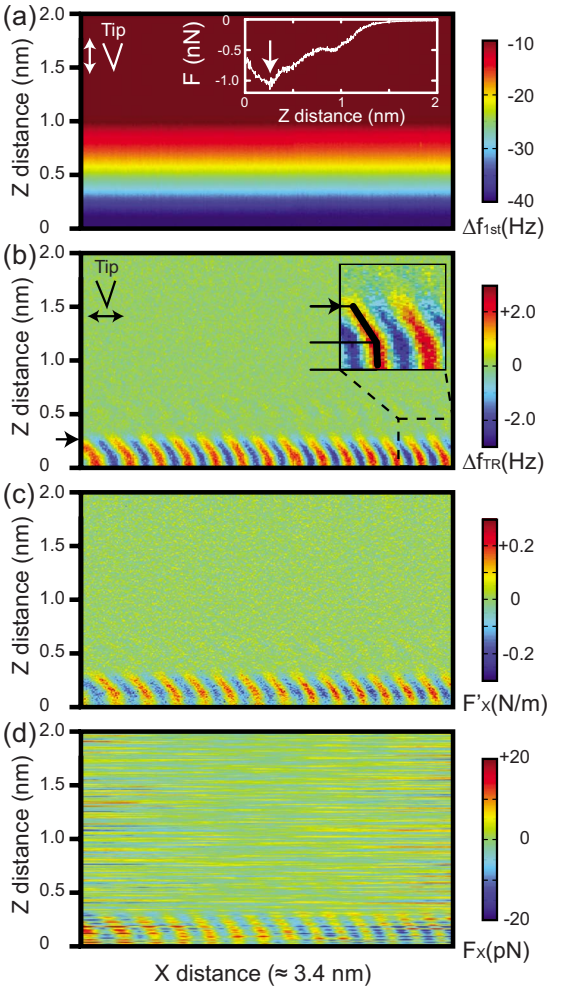

FIG. 5. (Color online) (a) Two-dimensional Δf_{1st} and (b) Δf_{TR} maps in the X-Z plane over a flat region. The insets show the interaction force, extracted from the measured Δf_{1st} in (a) and the magnified Δf_{TR} in (b). (c) Extracted lateral force gradient from the measured Δf_{TR}, using Eq. (6). (d) Lateral force obtained by integrating the lateral force gradient. The cantilever used was the same as that in Fig. 4 but the tip apex condition had changed. Measurement parameters; A_{1st}=15 pm, A_{TR}=38 pm, and V_{bias}=0.463 V.

cantilever with respect to the cantilever holder or the base of the microscope cannot be avoided but it is unlikely that these misalignments are the reason for a tilt angle as large as 30°. Presumably, the graphite surface was slightly deformed by the vertical attractive tip-sample interaction, causing a peculiar lateral force field, as observed in a previous study.[8] This angle becomes smaller upon a further decrease in the tip-sample distance. The distance corresponding to the most attractive vertical force (≈0.25 nm) is indicated with arrows in the insets of Figs. 5(a) and 5(b). At the closer distances, the vertical interaction force becomes less attractive. Therefore, the graphite surface was most likely less deformed below the most attractive tip-sample distance.

Changing the integration variable to $u=\cos\theta_{TR}$ in Eqs. (3) and (6), one notices that the resulting integrands have the same $(1-u^2)^{-1/2}$ singularities at the turning point $u=-1$ which dominates the results for large A_{1st}. In this case, the algorithm introduced by Dürig[40] to extract F_Z from Δf_{1st} can

also be applied to extract the lateral force gradient F'_X from Δf_{TR} as a function of the tip-sample distance,

$$F'_X = \frac{4k_{TR}}{A_{1st} f_{TR}} \int_z^\infty \sqrt{\frac{A_{1st}^3}{2(t-z)}} \frac{d\Delta f_{TR}(t)}{dt} dt. \quad (8)$$

Figure 5(c) shows the resulting lateral force gradient map. With decreasing tip-sample distance, the magnitude of the lateral force gradient first increases. In the X direction, a periodic sinusoidal variation of about ± 0.3 N/m is observed. This value is surprisingly large for an inert surface like graphite in the noncontact region but the small lattice spacing can enhance the modulation of the lateral force gradient for a given short-range vertical force. Near the shortest probed tip-sample distance set equal to 0 nm, a reduction in the lateral force gradient is observed. Since the short-range vertical interaction almost vanishes at that distance, as can be checked by subtracting the long-range interaction force presumed to act alone beyond about 0.7 nm in the inset of Fig. 5(a), the lateral force gradient is also reduced accordingly. This observation is also consistent with the simple calculation shows in Fig. 2(b). Since the lateral force varies sinusoidally to a good approximation, its average parallel to the surface at any tip-sample distance must vanish. Therefore, the lateral force can be simply obtained by integrating the extracted lateral force gradient along the X direction, then subtracting any residual offset obtained by averaging over a sufficient number of periods.[16] The finite torsional oscillation amplitude of 38 pm reduces the observed amplitude of lateral force by a factor of 89%, taking into account the lattice spacing of 246 pm.[35] Figure 5(d) shows the computed lateral force showing an extremely small but nevertheless distinct modulation below 20 pN. A similar treatment can be applied to extract the lateral variation in the interaction potential but, owing to the dead time between successive bimodal Z-dependent measurements, the noise in the raw data had to be removed by filtering.

Figure 6 shows the extracted lateral variation in the interaction potential showing an extremely weak corrugation of <3 meV. Irregular features at the right and left sides of the map are artifacts due to extensive filtering. The magnitude of the potential modulation at the distance corresponding to the maximum attractive force at RT is found to be 300 times smaller on graphite (0001) than on Si(111)-7×7(<1 eV) (Ref. 26) and seven times smaller than on NaCl(001) (<20 meV).[41] This extremely small lateral variation in the interaction potential is in line with the chemically inert nature of the perfect graphite (0001) surface.

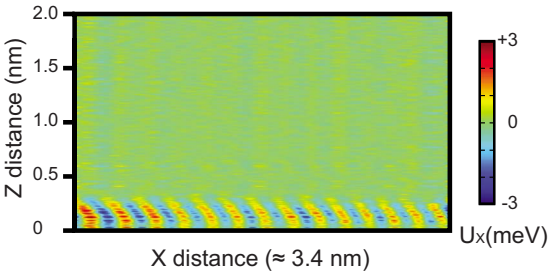

FIG. 6. (Color online) (a) Lateral interaction potential variation map U_X obtained by integrating the lateral force shown in Fig. 5(d) in the X direction.

V. CONCLUSIONS

We have shown that bimodal DFM using the first-flexural and torsional resonance modes enables extremely sensitive high-resolution measurements of atomic-scale lateral forces. Since only the site-dependent short-range tip-sample interaction gives rise to such forces on nominally flat areas, the achieved resolution is drastically improved compared to conventional DFM. This enhanced detection sensitivity is predicted by theory, validated by model calculations and convincingly demonstrated by lattice-resolved images and distance-dependent maps of the torsional resonance frequency shift recorded in the attractive force range on graphite (0001) at room temperature. Similar maps of the lateral force gradient, of the lateral force and of lateral corrugation of the interaction potential, showing distinct variations with the lattice periodicity have been obtained. The lateral force was calculated by differentiating the measured potential via the vertical interaction.[42,43] To compare the indirect measurement, bimodal DFM, presented in this paper, has an advantage to increase the sensitivity of the lateral force detection.

ACKNOWLEDGMENTS

This work was supported in part by the Swiss National Science Foundation, the ESF EUROCORE program FANAS and by the Swiss National Center of Competence "Nanoscale Science." The author (S.K.) would like to thank Naruo Sasaki for many helpful discussions.

*shigeki.kawai@unibas.ch
†Present address: Research Centre for Nanometer-Scale Science and Advanced Materials (NANOSAM), Faculty of Physics, Astronomy, and Applied Computer Science, Jagiellonian University, Reymonta 4, 30-059 Krakow, Poland.

[1] L. Gross, F. Mohn, N. Moll, P. Liljeroth, and G. Meyer, Science **325**, 1110 (2009).
[2] T. R. Albrecht, P. Grütter, D. Horne, and D. Rugar, J. Appl. Phys. **69**, 668 (1991).
[3] W. Allers, A. Schwarz, U. D. Schwarz, and R. Wiesendanger, Appl. Surf. Sci. **140**, 247 (1999).
[4] A. Schwarz, U. D. Schwarz, S. Langkat, H. Hölscher, W. Allers, and R. Wiesendanger, Appl. Surf. Sci. **188**, 245 (2002).
[5] S. Hembacher, F. J. Giessibl, J. Mannhart, and C. F. Quate, Proc. Natl. Acad. Sci. U.S.A. **100**, 12539 (2003).
[6] S. Hembacher, F. J. Giessibl, and J. Mannhart, Science **305**, 380 (2004).
[7] S. Hembacher, F. J. Giessibl, J. Mannhart, and C. F. Quate, Phys.

Rev. Lett. **94**, 056101 (2005).
[8] B. J. Albers, T. C. Schwendemann, M. Z. Baykara, N. Pilet, M. Liebmann, E. I. Altman, and U. D. Schwarz, Nat. Nanotechnol. **4**, 307 (2009).
[9] G. Binnig, H. Fuchs, C. Gerber, H. Rohrer, E. Stoll, and E. Tosatti, Europhys. Lett. **1**, 31 (1986).
[10] S.-I. Park and C. F. Quate, Appl. Phys. Lett. **48**, 112 (1986).
[11] S. Kawai and H. Kawakatsu, Phys. Rev. B **79**, 115440 (2009).
[12] C. M. Mate, G. M. McClelland, R. Erlandsson, and S. Chiang, Phys. Rev. Lett. **59**, 1942 (1987).
[13] O. Pfeiffer, R. Bennewitz, A. Baratoff, E. Meyer, and P. Grütter, Phys. Rev. B **65**, 161403(R) (2002).
[14] F. J. Giessibl, M. Herz, and J. Mannhart, Proc. Natl. Acad. Sci. U.S.A. **99**, 12006 (2002).
[15] S. Kawai, S. Kitamura, D. Kobayashi, and H. Kawakatsu, Appl. Phys. Lett. **87**, 173105 (2005).
[16] S. Kawai, N. Sasaki, and H. Kawakatsu, Phys. Rev. B **79**, 195412 (2009).
[17] M. Heyde, M. Sterrer, H. P. Rust, and H. J. Freund, Nanotechnology **17**, S101 (2006).
[18] T. R. Rodríguez and R. García, Appl. Phys. Lett. **84**, 449 (2004).
[19] R. García, R. Magerle, and R. Perez, Nature Mater. **6**, 405 (2007).
[20] J. R. Lozano and R. García, Phys. Rev. Lett. **100**, 076102 (2008).
[21] S. Kawai, T. Glatzel, S. Koch, B. Such, A. Baratoff, and E. Meyer, Phys. Rev. Lett. **103**, 220801 (2009).
[22] F. Giessibl, H. Bielefeldt, S. Hembacher, and J. Mannhart, Ann. Phys. **10**, 887 (2001).
[23] S. Kawai, S. Kitamura, D. Kobayashi, S. Meguro, and H. Kawakatsu, Appl. Phys. Lett. **86**, 193107 (2005).
[24] S. Kawai and H. Kawakatsu, Appl. Phys. Lett. **88**, 133103 (2006).
[25] S. Kawai, F. Rose, T. Ishii, and H. Kawakatsu, J. Appl. Phys. **99**, 104312 (2006).
[26] Y. Sugimoto, T. Namikawa, K. Miki, M. Abe, and S. Morita, Phys. Rev. B **77**, 195424 (2008).
[27] F. J. Giessibl, Phys. Rev. B **56**, 16010 (1997).
[28] N. Sasaki and M. Tsukada, Jpn. J. Appl. Phys. **37**, L533 (1998).
[29] R. Pérez, I. Štich, M. C. Payne, and K. Terakura, Phys. Rev. B **58**, 10835 (1998).
[30] M. Guggisberg, M. Bammerlin, C. Loppacher, O. Pfeiffer, A. Abdurixit, V. Barwich, R. Bennewitz, A. Baratoff, E. Meyer, and H. J. Güntherodt, Phys. Rev. B **61**, 11151 (2000).
[31] J. Israelachvili, *Intermolecular and Surface Forces*, 2nd ed. (Academic, London, 1991).
[32] A. Oral, R. A. Grimble, H. O. Özer, P. M. Hoffmann, and J. B. Pethica, Appl. Phys. Lett. **79**, 1915 (2001).
[33] L. Howald, E. Meyer, R. Lüthi, H. Haefke, R. Overney, H. Rudin, and H. J. Güntherodt, Appl. Phys. Lett. **63**, 117 (1993).
[34] G. H. Simon, M. Heyde, and H.-P. Rust, Nanotechnology **18**, 255503 (2007).
[35] N. Sasaki, S. Kawai, and H. Kawakatsu, Phys. Rev. B **80**, 193402 (2009).
[36] I. Horcas, R. Fernandez, J. Gomez-Rodriguez, J. Colchero, J. Gomez-Herrero, and A. Baro, Rev. Sci. Instrum. **78**, 013705 (2007).
[37] S. Ciraci, A. Baratoff, and I. P. Batra, Phys. Rev. B **41**, 2763 (1990).
[38] H. Hölscher, W. Allers, U. D. Schwarz, A. Schwarz, and R. Wiesendanger, Phys. Rev. B **62**, 6967 (2000).
[39] J. E. Sader and S. P. Jarvis, Appl. Phys. Lett. **84**, 1801 (2004).
[40] U. Dürig, Appl. Phys. Lett. **75**, 433 (1999).
[41] A. Schirmeisen, D. Weiner, and H. Fuchs, Phys. Rev. Lett. **97**, 136101 (2006).
[42] A. Schwarz, H. Hölscher, S. M. Langkat, and R. Wiesendanger, in *Scanning Tunneling Microscopy/Spectroscopy and Related Techniques*, edited by P. M. Koenraad and M. Kemerink, AIP Conf. Proc. No. 696 (AIP, New York, 2003), p. 68.
[43] M. Ternes, C. P. Lutz, C. F. Hirjibehedin, F. J. Giessibl, and A. J. Heinrich, Science **319**, 1066 (2008).